

Ambient noise correlation on the Amery Ice Shelf, East Antarctica

Zhongwen Zhan,^{*} Victor C. Tsai, Jennifer M. Jackson and Don Helmberger

Seismological Laboratory, California Institute of Technology, 1200 E. California Blvd., Pasadena, CA 91125, USA. E-mail: zwzhan@uclsd.edu

Accepted 2013 November 28. Received 2013 November 27; in original form 2013 August 16

SUMMARY

The structure of ice shelves is important for modelling the dynamics of ice flux from the continents to the oceans. While other, more traditional techniques provide many constraints, passive imaging with seismic noise is a complementary tool for studying and monitoring ice shelves. As a proof of concept, here we study noise cross-correlations and autocorrelations on the Amery Ice Shelf, East Antarctica. We find that the noise field on the ice shelf is dominated by energy trapped in a low-velocity waveguide caused by the water layer below the ice. Within this interpretation, we explain spectral ratios of the noise cross-correlations as *P*-wave resonances in the water layer, and obtain an independent estimate of the water-column thickness, consistent with other measurements. For stations with noise dominated by elastic waves, noise autocorrelations also provide similar results. High-frequency noise correlations also require a 50-m firn layer near the surface with *P*-wave velocity as low as 1 km s⁻¹. Our study may also provide insight for future planetary missions that involve seismic exploration of icy satellites such as Titan and Europa.

Key words: Interferometry; Guided waves; Antarctica.

INTRODUCTION

Ice shelves are important interfaces between grounded ice sheets and oceans, and contribute to the majority of grounded ice loss either through basal melting or iceberg calving. Accurate modelling of ice shelf dynamics (e.g. sub-ice circulation and ice flow modelling) requires high-resolution ice drafts and water-column thicknesses, which are usually poorly constrained for ice shelves. Currently, ice drafts and water-column thicknesses are constrained mostly from digital elevation modelling (Fricker *et al.* 2005), tidal modelling (Hemer *et al.* 2006; Galton-Fenzi *et al.* 2008), and sparse active seismic surveys and drillings (McMahon & Lackie 2006; Craven *et al.* 2009). It is therefore of interest whether other methods can contribute additional and/or better constraints. One method that has received little attention in cryospheric studies is passive imaging with ambient seismic noise. Passive imaging can be applied over large areas at a low cost and without direct sampling, and has been widely used to study crustal structure around the globe in recent years (e.g. Shapiro *et al.* 2005; Yao *et al.* 2006; Lin *et al.* 2008), including in Antarctica (Pyle *et al.* 2010). However, most of these studies are located in the interior of the continent and concentrate on the structure of the crust or upper mantle using long-period ($T > 5$ s) surface waves. To our knowledge, there has not been any report of small-scale noise correlation on ice shelves. The reason for

this may be twofold. First, due to the harsh environment and difficult logistics, there is little continuous data available on ice shelves. Second, the ice-water-rock setting with a strong low-velocity layer is significantly different from ordinary crustal structure and could affect the convergence and interpretation of noise cross-correlation functions (NCFs). To address the question of what can be gained with such an approach, we apply noise correlation methods to the Amery Ice Shelf on the east coast of Antarctica (Fig. 1A), where a number of seismic instruments were deployed for multiple years near the tip of the Loose Tooth Rift system to monitor its growth (Bassis *et al.* 2005; Fricker *et al.* 2005; Bassis *et al.* 2007; Fig. 1B). Near the site, the thicknesses of the ice and water layers are about 300 and 500 m, respectively (Fricker *et al.* 2005; Galton-Fenzi *et al.* 2008; Fig. 2). One question we explore is whether we can retrieve this structural information from noise correlations.

This experiment also serves as a proof of concept for planetary applications of the noise correlation method on icy satellites. For example, a variety of evidence suggests that there may exist subsurface liquid oceans on Europa (e.g. Carr *et al.* 1998; Kivelson *et al.* 2000) and Titan (e.g. Tobie *et al.* 2006; Lunine & Lorenz 2009; Castillo-Rogez & Lunine 2010). The thicknesses of the ice and liquid layers, which are important for understanding icy satellite dynamics, are still uncertain. Different kinds of seismic experiments have been proposed to improve estimates in future missions (e.g. Kovach & Chyba 2001; Lee *et al.* 2003; Panning *et al.* 2006; Jackson *et al.* 2010; Tsai 2010a). In particular, the emerging noise correlation method is attractive for planetary missions because it potentially provides surface-wave (e.g. Shapiro *et al.* 2005) and body-wave (e.g. Zhan *et al.* 2010; Poli *et al.* 2012; Lin *et al.* 2013) Green's

^{*}Now at Institute of Geophysics and Planetary Physics, Scripps Institution of Oceanography, University of California, San Diego, 9500 Gilman Dr., La Jolla, CA 92093, USA

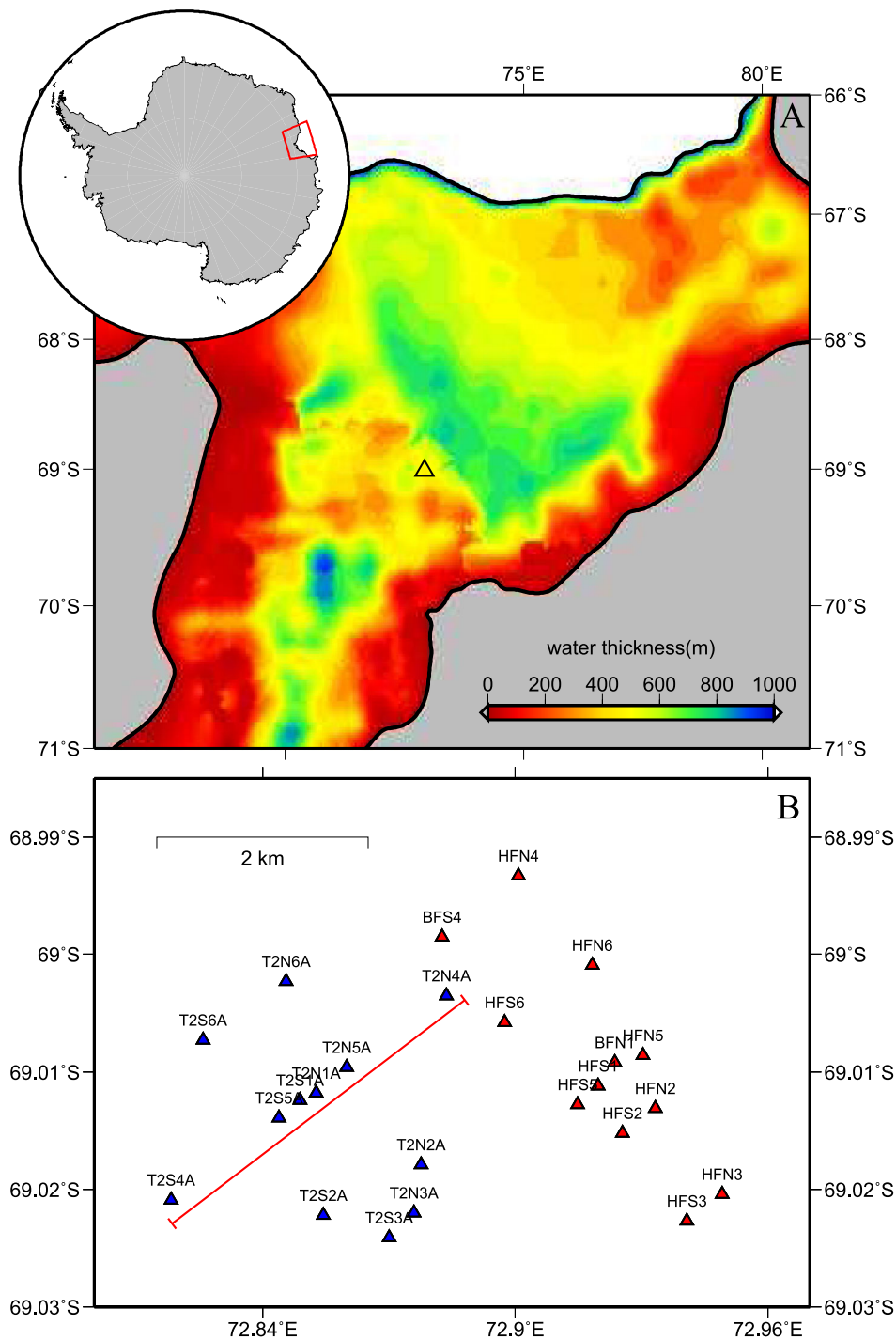


Figure 1. (A) Map of the Amery Ice Shelf and water-column thickness. The triangle marks the location of the seismic deployment. (B) Station distribution map. Blue triangles and red triangles show the stations deployed in 2005 and 2007, respectively. The red line denotes the profile whose NCFs are shown in Fig. 3. In both years, the instruments surround the same ice area, but the ice has advected ~ 2 km (to the NE) in the 2 yr between deployments.

functions without seismic events. For example, [Larose *et al.* \(2005\)](#) applied the noise correlation method to lunar data and constrained the near-surface (top 10 m) seismic structure. Recently, [Tibuleac & von Seggern \(2012\)](#) and [Gorbatov *et al.* \(2013\)](#) also reported reflected crustal phases from noise autocorrelations on individual stations. Because it is difficult to deploy more than one seismic station in planetary missions, the noise autocorrelation method might be more practical than the cross-correlation method. With a sim-

ilar ice–liquid–solid structural setting, the Amery Ice Shelf is an ideal test ground for the application of noise cross-correlation and autocorrelation methods on icy satellites.

DATA AND METHOD

Fig. 1(B) shows the locations of the three-component short-period (1–10 Hz) instruments deployed during the 2005 and 2007 field

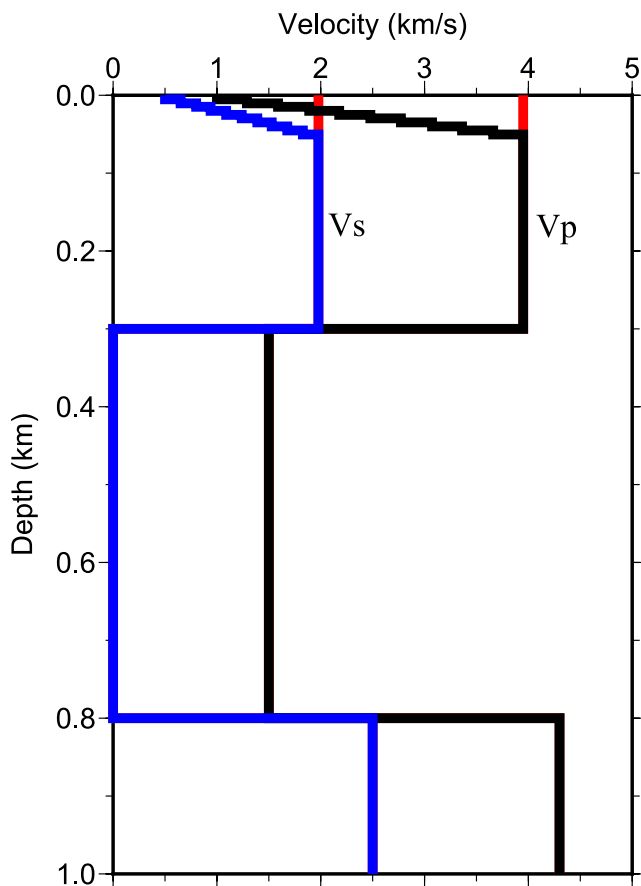


Figure 2. The 1-D P - and S -wave velocity models used to compute synthetic Green's functions. Differences between the two 1-D models with or without the top 50-m firn layer are highlighted by the red segments.

seasons. Both campaigns (Bassis *et al.* 2007) were active for about 2 months during the Antarctic summer. Because of the different environment and frequency band from most noise correlation studies, we modified some of the common procedures (e.g. Bensen *et al.* 2007; Zhan *et al.* 2011) to calculate the nine-component NCFs (E, N, Z with E, N, Z) for all station pairs. We first remove instrumental responses and cut the data into 10-min segments. Because signals from earthquakes are weak in the frequency band of 1–10 Hz, here we do not use temporal normalization to remove earthquakes. To preserve the amplitude spectrum, especially for autocorrelations, we also do not apply spectral whitening to the waveforms. The two stations' waveforms are cross correlated for each segment and then stacked with normalized maximum amplitudes. The use of very short 10-min segments and normalized stacking achieves the equivalent of the temporal normalization used in most noise correlation studies to remove earthquakes, and may be important in the presence of occasional icequakes.

NOISE CROSS-CORRELATIONS IN TIME DOMAIN

Although the elastic structure of the ice shelf near the site can be estimated with other methods (e.g. Vaughan 1995), the NCFs produced here provide the first direct *in situ* measurement of ice shelf elastic structure. Elastic structure is inferred from the NCFs by comparing the observations with synthetic Green's functions produced for various assumed structures using a frequency-wavenumber method

(Zhu & Rivera 2002) to compute the synthetic Green's functions due to a surface point force. Using borehole measurements, Craven *et al.* (2009) show that the ice shelf consists of a ~ 50 m firn layer on top of a ~ 250 m continental meteoric and marine ice layer. Following Wittlinger & Farra (2012), we set the V_p and V_s to be 3.95 and 2 km s^{-1} , respectively, for both the meteoric and marine ice layer. The velocities in the firn layer are poorly constrained and V_p can be as low as 0.5 km s^{-1} (Albert 1998), and we therefore test two different models, one without a slow firn layer, and one with a slow layer of constant gradient and V_p/V_s ratio of 2 (Fig. 2). For the latter model, we adjust the absolute V_p on the surface to best fit the seismic data.

We first compare the NCFs along a NE-SW profile (red line in Fig. 1B) with the synthetic Green's functions in the 5–10 Hz frequency band (Figs 3A and B). We rotated the EN-EN NCFs into radial-radial (RR) components and summed the positive and negative sides. We see clear Rayleigh waves in the NCFs (dashed line in Fig. 3A) propagating at a speed of about 1.5 km s^{-1} , much slower than the synthetic Rayleigh waves of the 1-D homogeneous ice model (without a slow firn layer), as shown in red in Fig. 3(B). To fit the observed Rayleigh waves, we adjust the 1-D model with a slow firn layer to have a surface V_p of 1 km s^{-1} and plot the synthetics in black in Fig. 3(B). We note that if a more complex velocity structure were allowed, there would be tradeoffs between the various parameters, including the thickness of the slow layer and its velocity anomaly.

In the 5–10 Hz frequency band, the observed Rayleigh waves are only sensitive to depths shallower than about 100 m, significantly shorter than the ice thickness, and therefore do not have sensitivity to the ice-water interface. To sample the interface, we need to study NCFs at lower frequencies. For the same station pairs at 1–5 Hz, the synthetic Green's functions are similar for the two 1-D models because they are only different in the thin top layer. However, we find that the NCFs do not resemble these synthetic Green's functions (Figs 3C and D). In fact, the observed NCFs clearly cannot be represented by a Green's function because they violate causality. The dashed line in Fig. 3(D) marks the onset of the synthetics, and the P , S and surface waves must arrive after this dashed line due to causality. On the other hand, the observed NCFs are acausal, with most of their energy arriving before or around the same time as the dashed line shown in Fig. 3(C). This comparison is also true for other station pairs. Therefore, it is not possible to interpret the NCFs solely as being Green's functions between stations, and we must rely on an alternative interpretation of the NCFs to retrieve further structural information.

SPECTRAL RATIOS OF NOISE CROSS-CORRELATIONS

Although the 1–5 Hz NCFs in the time domain are difficult to interpret, we find that the spectral ratios of NCFs on different components still contain useful information about the velocity structure. With the three-component stations, we have nine components of the NCFs (ZNE-ZNE) for each station pair. We first estimate the NCF amplitude spectra for all components and then take their spectral ratios with the ZZ component (ZZ/XY, where X and Y can be Z, N or E). Fig. 4 shows the average spectral ratios over all station pairs for each component in 2007. For all the components (except ZZ/ZZ which is 1 by definition), we observe regularly spaced peaks at about every 1.5 Hz up to about 6 Hz. These peaks are stronger on the components involving only East or North (Figs 4E, F, H, and I).

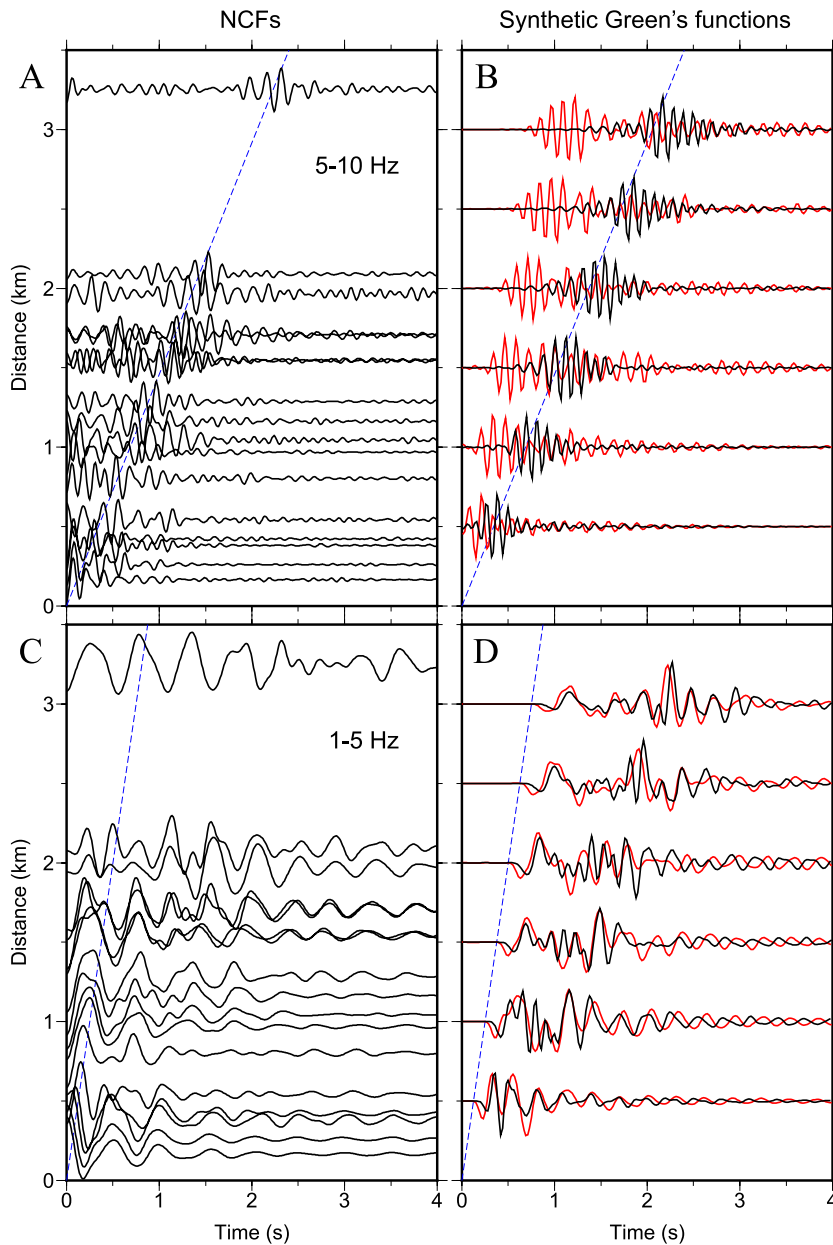


Figure 3. NCFs in the time domain (A, C) and comparisons with synthetic Green's functions (B, D). The top and bottom panels are for the frequency bands 5–10 and 1–5 Hz, respectively. In (B, D), the red and black synthetics are computed with the 1-D models without and with the firn layer, respectively.

The observed peaks in the NCF spectral ratios are approximately equally spaced in frequency (a phenomenon typical for resonating systems), and imply more coherent waves on the vertical components than the horizontal components at these frequencies.

We interpret the observed peaks in Fig. 4 as P -wave resonances in the water layer (Fig. 5). As shown in Fig. 2, the water layer sandwiched between the ice and rock layers is a strong low-velocity waveguide with little attenuation (high Q). The water layer therefore traps seismic waves and creates a diffuse wavefield inside it. For P waves traveling inside the water layer, the critical angle is about 22° for the top ice-water interface and smaller ($\approx 20^\circ$) for the bottom water-rock interface. Therefore, waves in the water layer with incident angles larger than 22° will be completely reflected back to the water and are not recorded on the free surface under the assumption of geometrical ray theory. Waves with incident angles (θ in Fig. 5) smaller than the critical angle can leak into the ice layer and reach

the stations at the free surface. Due to the slow firn layer on top, the transmitted P waves will bend steeper towards the surface, and reach the stations with incident angles smaller than the $\theta \leq 22^\circ$ in the water layer (Fig. 5). These steeply traveling P waves will cause stronger ground motion on the vertical components than the horizontal components. Because these transmitted P waves have travelled nearly vertically ($\theta \leq 22^\circ$) inside the water layer, we can calculate the resonance frequencies as $f_n = n \frac{V_p}{2H}$, where $n = 1, 2, 3, \dots$, H is the water-column thickness, and assuming θ is small. Given $V_p \approx 1.5 \text{ km s}^{-1}$, we derive $H \approx 500 \text{ m}$ from the resonance peaks at 1.5, 3, 4.5 and 6 Hz (Fig. 4), consistent with the previous measurements shown in Fig. 1(A) (Galton-Fenzi *et al.* 2008). Considering uncertainties in the measured resonance frequencies due to smooth peaks ($\sim 0.1 \text{ Hz}$, Fig. 4) and in the assumed P -wave speed in water (~ 1 per cent), our estimate of the water-column thickness H would have an uncertainty of about 40 m.

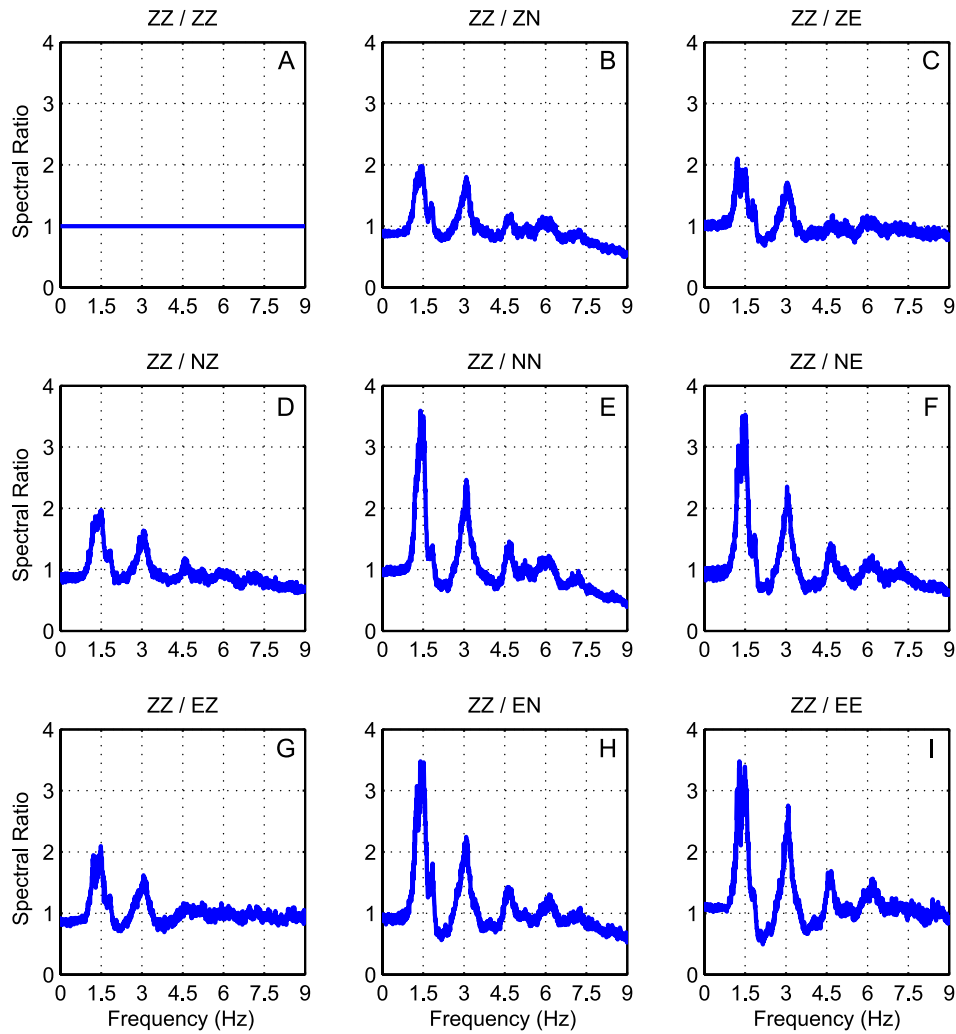


Figure 4. Average NCF spectral ratios for the year 2007. The title of each panel shows the components in format ZZ/XY, where X and Y can be one of E, N, Z.

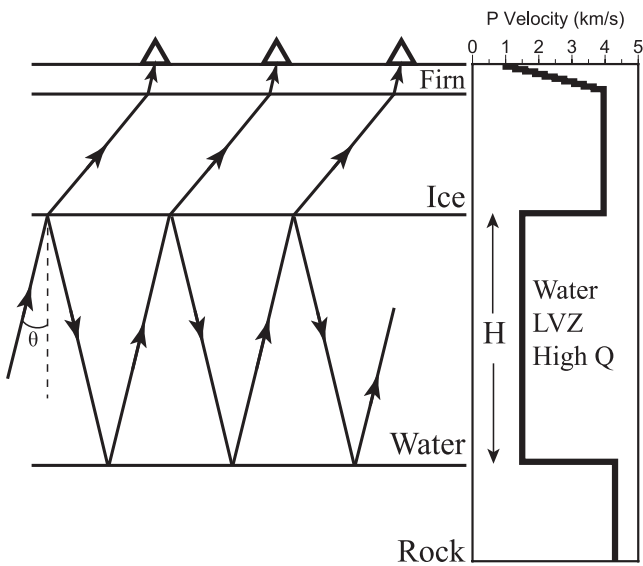


Figure 5. Illustration of how trapped waves in the slow water layer propagate to the free surface. The 1-D *P*-wave velocity model is plotted to the right as reference. See the text for more details.

With the new interpretation of the NCF spectral ratios described above, we can now explain the observed NCFs in the time domain (Fig. 3C). Because the coherent 1–5 Hz noise at the stations are dominated by the nearly vertical *P* waves from the water layer, the NCFs will have most of their signal near zero lag and will not resemble the Green’s functions between the stations (Fig. 3), which would have been retrieved if the noise field were fully diffuse (Lobkis & Weaver 2001). Note that the NCFs’ failure to converge to Green’s functions is directly related to the structure itself, that is the strong low-velocity water layer causes the noise field to be non-diffuse. In order for the noise field to remain diffuse with this structure, a very specific non-uniform distribution of noise sources would be required (Tsai 2010b). The observed resonance peaks decay as frequency increases (Fig. 4) and are small at about 6 Hz. This may be caused by stronger seismic scattering or attenuation at higher frequencies. For the frequency band of 5–10 Hz, the coherent noise field may therefore be more diffuse than in the 1–5 Hz band, and the observed NCFs resemble the Rayleigh-wave Green’s functions (Fig. 3).

NOISE AUTOCORRELATIONS

Cross-correlation between two stations emphasizes the coherent noise and reduces the incoherent noise relative to the raw noise

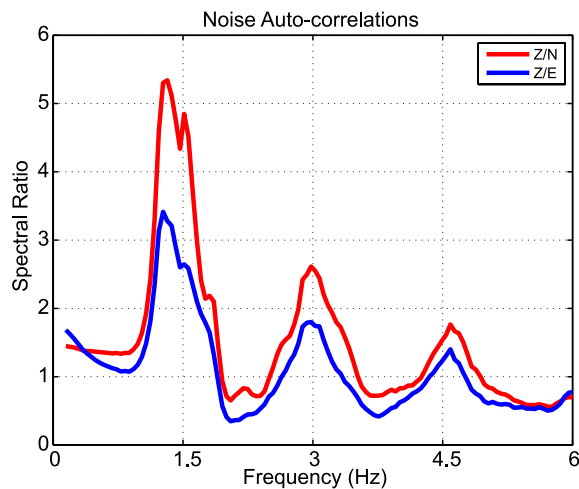


Figure 6. Spectral ratios of noise autocorrelations at station BFN1 in 2007. The red and blue curves are for ratios between vertical and north or east, respectively.

measurements. The coherent seismic noise in Antarctica may consist of seismic waves generated by ocean waves, winds, ice cracking and biomechanical processes. As discussed in the previous section, the coherent noise on the ice shelf is dominated by the P waves from the water layer such that we can clearly identify the water-layer resonance peaks from the NCFs. In contrast, the incoherent noise may consist of mechanical noise, electronic noise, inelastic deformation or any other perturbations that do not propagate from one station to another. We find that the noise levels at the stations used in this study are quite different (see Figs S1 and S2), with most stations clearly dominated by incoherent noise. Due to these high levels of incoherent noise, the resonances can only be easily identified after cross-correlations among stations, which enhance the coherent noise. However, if the incoherent noise is weaker than the coherent noise at some stations, we should still be able to observe the resonance peaks in the spectral ratios of the three-component autocorrelations. Indeed, for one broadband station during the 2007 deployment, we can observe the same resonances in the spectral ratios between the vertical and two horizontal components (Fig. 6) as in cross-correlations (Fig. 4). Note that the autocorrelation spectra of individual components are affected by both source spectra and structure, and therefore do not display the resonance clearly (Fig S3). As shown by an example in Fig. S4, stations dominated by incoherent noise do not present resonance peaks in the spectral ratios either, because autocorrelation cannot reduce the incoherent noise. These successful and failed examples suggest that noise autocorrelations can also be used to study ice shelf structure but requires a careful setup (e.g. three-component, instrument type, wind isolation, ground coupling) for lower levels of incoherent noise. Since the autocorrelation method is particularly attractive for planetary missions with a single station, these factors should be considered in the design of such experiments.

CONCLUSIONS

In this paper, we have studied noise cross-correlations and autocorrelations on the Amery Ice Shelf. For the frequency band 5–10 Hz, we retrieved Rayleigh-wave Green's functions between stations, and determined that P -wave velocities in the top 50-m firn layer (down to 1 km/s) are significantly slower than typical ice P -wave velocities. For the frequency band 1–5 Hz, we find that the NCFs do not

converge to the Green's functions. Instead, we explain the observations as resulting from a significantly non-diffuse noise field caused by the low-velocity waveguide of the water layer sandwiched between the ice and rock layers. Under this new interpretation, we explain the observed peaks in the NCF spectral ratios as P -wave resonances in the water layer, and estimate the water-column thickness. For stations with low levels of incoherent noise, noise autocorrelations also provide a consistent estimate of water thickness. These results can help in the design of future passive seismic experiments to estimate and monitor the structure of ice shelves and water-column thicknesses. Our study may also provide insight for the design of future missions involving seismic exploration of other planetary bodies. In particular, the study presented here serves as a proof of concept for planetary applications of the noise correlation method on icy satellites, such as Titan and Europa.

ACKNOWLEDGEMENTS

We thank Fan-Chi Lin, Robert Clayton and Mark Simons for helpful discussions. We thank the editor Michael Ritzwoller and two anonymous reviewers for their comments that improved the manuscript. The seismic data is from the Incorporated Research Institutions for Seismology (IRIS) and David Heeszel and Helen Fricker helped with the seismic data. This work is supported in part by the Keck Institute for Space Studies (JMJ).

REFERENCES

- Albert, D.G., 1998. Theoretical modeling of seismic noise propagation in firn at the South Pole, Antarctica, *Geophys. Res. Lett.*, **25**, 4257–4260.
- Bassis, J.N., Coleman, R., Fricker, H. & Minster, J., 2005. Episodic propagation of a rift on the Amery Ice Shelf, East Antarctica, *Geophys. Res. Lett.*, **32**, L06502, doi:10.1029/2004GL022048.
- Bassis, J.N., Fricker, H.A., Coleman, R., Bock, Y., Behrens, J., Darnell, D., Okal, M. & Minster, J.-B., 2007. Seismicity and deformation associated with ice-shelf rift propagation, *J. Glaciol.*, **53**, 523–536.
- Bensen, G., Ritzwoller, M., Barmin, M., Levshin, A., Lin, F., Moschetti, M., Shapiro, N. & Yang, Y., 2007. Processing seismic ambient noise data to obtain reliable broad-band surface wave dispersion measurements, *Geophys. J. Int.*, **169**, 1239–1260.
- Carr, M.H. *et al.*, 1998. Evidence for a subsurface ocean on Europa, *Nature*, **391**, 363–365.
- Castillo-Rogez, J.C. & Lunine, J.I., 2010. Evolution of Titan's rocky core constrained by Cassini observations, *Geophys. Res. Lett.*, **37**, L20205, doi:10.1029/2010GL044398.
- Craven, M., Allison, I., Fricker, H.A. & Warner, R., 2009. Properties of a marine ice layer under the Amery Ice Shelf, East Antarctica, *J. Glaciol.*, **55**, 717–728.
- Fricker, H., Young, N., Coleman, R., Bassis, J. & Minster, J.B., 2005. Multi-year monitoring of rift propagation on the Amery Ice Shelf, East Antarctica, *Geophys. Res. Lett.*, **32**, L02502, doi:10.1029/2004GL021036.
- Galton-Fenzi, B., Maraldi, C., Coleman, R. & Hunter, J., 2008. The cavity under the Amery Ice Shelf, East Antarctica, *J. Glaciol.*, **54**, 881–887.
- Gorbatov, A., Saygin, E. & Kennett, B., 2013. Crustal properties from seismic station autocorrelations, *Geophys. J. Int.*, **192**, 861–870.
- Hemer, M., Hunter, J. & Coleman, R., 2006. Barotropic tides beneath the Amery Ice Shelf, *J. geophys. Res.*, **111**, C11008, doi:10.1029/2006JC003622.
- Jackson, J., Zhan, Z., Clayton, R., Helmberger, D. & Tsai, V., 2010. Ambient seismic noise applications for Titan. in *Proceedings of the AGU Fall Meeting*, San Francisco, CA, 13–17 Dec.
- Kivelson, M.G., Khurana, K.K., Russell, C.T., Volwerk, M., Walker, R.J. & Zimmer, C., 2000. Galileo magnetometer measurements: a stronger case for a subsurface ocean at Europa, *Science*, **289**, 1340–1343.

- Kovach, R.L. & Chyba, C.F., 2001. Seismic detectability of a subsurface ocean on Europa, *Icarus*, **150**, 279–287.
- Larose, E., Khan, A., Nakamura, Y. & Campillo, M., 2005. Lunar subsurface investigated from correlation of seismic noise, *Geophys. Res. Lett.*, **32**, L16201, doi:10.1029/2005GL023518.
- Lee, S., Zanolin, M., Thode, A.M., Pappalardo, R.T. & Makris, N.C., 2003. Probing Europa's interior with natural sound sources, *Icarus*, **165**, 144–167.
- Lin, F.C., Moschetti, M.P. & Ritzwoller, M.H., 2008. Surface wave tomography of the western United States from ambient seismic noise: Rayleigh and Love wave phase velocity maps, *Geophys. J. Int.*, **173**, 281–298.
- Lin, F.C., Tsai, V.C., Schmandt, B., Duputel, Z. & Zhan, Z., 2013. Extracting seismic core phases with array interferometry, *Geophys. Res. Lett.*, **40**, 1049–1053.
- Lobkis, O.I. & Weaver, R.L., 2001. On the emergence of the Green's function in the correlations of a diffuse field, *J. acoust. Soc. Am.*, **110**, 3011.
- Lunine, J.I. & Lorenz, R.D., 2009. Rivers, lakes, dunes, and rain: Crustal processes in Titan's methane cycle, *Annu. Rev. Earth Planet. Sci.*, **37**, 299–320.
- McMahon, K.L. & Lackie, M.A., 2006. Seismic reflection studies of the Amery Ice Shelf, East Antarctica: delineating meteoric and marine ice, *Geophys. J. Int.*, **166**, 757–766.
- Panning, M., Lekic, V., Manga, M., Cammarano, F. & Romanowicz, B., 2006. Long-period seismology on Europa: 2. Predicted seismic response, *J. geophys. Res.*, **111**, E12008, doi:10.1029/2006JE002712.
- Poli, P., Campillo, M. & Pedersen, H., 2012. Body-wave imaging of earth's mantle discontinuities from ambient seismic noise, *Science*, **338**, 1063–1065.
- Pyle, M.L., Wiens, D.A., Nyblade, A.A. & Anandakrishnan, S., 2010. Crustal structure of the Transantarctic Mountains near the Ross Sea from ambient seismic noise tomography, *J. geophys. Res.*, **115**, B11310, doi:10.1029/2009JB007081.
- Shapiro, N.M., Campillo, M., Stehly, L. & Ritzwoller, M.H., 2005. High-resolution surface-wave tomography from ambient seismic noise, *Science*, **307**, 1615–1618.
- Tibuleac, I.M. & von Seggern, D., 2012. Crust–mantle boundary reflectors in Nevada from ambient seismic noise autocorrelations, *Geophys. J. Int.*, **189**, 493–500.
- Tobie, G., Lunine, J.I. & Sotin, C., 2006. Episodic outgassing as the origin of atmospheric methane on Titan, *Nature*, **440**, 61–64.
- Tsai, V.C., 2010a. One-station seismology without traditional seismic sources, in *Proceedings of the AGU Fall Meeting*, San Francisco, CA, 13–17 Dec.
- Tsai, V.C., 2010b. The relationship between noise correlation and the Green's function in the presence of degeneracy and the absence of equipartition, *Geophys. J. Int.*, **182**, 1509–1514.
- Vaughan, D.G., 1995. Tidal flexure at ice shelf margins, *J. geophys. Res.*, **100**, 6213–6224.
- Wittlinger, G. & Farra, V., 2012. Observation of low shear wave velocity at the base of the polar ice sheets: evidence for enhanced anisotropy, *Geophys. J. Int.*, **190**, 391–405.
- Yao, H., van Der Hilst, R.D. & De Hoop, M.V., 2006. Surface-wave array tomography in SE Tibet from ambient seismic noise and two-station analysis—I. Phase velocity maps, *Geophys. J. Int.*, **166**, 732–744.
- Zhan, Z., Ni, S., Helmberger, D.V. & Clayton, R.W., 2010. Retrieval of Moho-reflected shear wave arrivals from ambient seismic noise, *Geophys. J. Int.*, **182**, 408–420.
- Zhan, Z., Wei, S., Ni, S. & Helmberger, D., 2011. Earthquake centroid locations using calibration from ambient seismic noise, *Bull. seism. Soc. Am.*, **101**, 1438–1445.
- Zhu, L. & Rivera, L.A., 2002. A note on the dynamic and static displacements from a point source in multilayered media, *Geophys. J. Int.*, **148**, 619–627.

SUPPORTING INFORMATION

Additional Supporting Information may be found in the online version of this article:

Figure S1. Ambient seismic noise levels in dB relative to velocity power at two stations, HFN3 and BFN1, (Fig. 1B). Both stations have three components (east, north, vertical; or ENZ) but different types of instruments (EP, HH). The drop in power at frequencies less than 2 Hz is caused by a high-pass filter to the short-period instruments. Note that at all frequencies, BFN1 is 30 dB quieter than HFN3, although they are separated by less than 2 km. Since the ambient noise field is unlikely to vary by 30 dB within 2 km, we believe that HFN3's records are probably dominated by incoherent noise, that is not dominated by coherent elastic waves.

Figure S2. A 10-min raw noise records from HFN3 and BFN1 at the same scale.

Figure S3. Autocorrelation spectra for BFN1's three components (Z, N, E). These spectra do not show the resonances because they are controlled by both noise source amplitude and structure. The spectral ratios cancel the source term and highlight the structure term with resonance peaks (Fig. 6).

Figure S4. Autocorrelation spectral ratios for station HFN3, the noisier station shown in Fig. S1. Because incoherent noise dominates the noise records and autocorrelation does not enhance the coherent noise, the resonance peaks are not visible.

(<http://gji.oxfordjournals.org/lookup/suppl/doi:10.1093/gji/ggt488/-/DC1>)

Please note: Oxford University Press are not responsible for the content or functionality of any supporting materials supplied by the authors. Any queries (other than missing material) should be directed to the corresponding author for the article.